Photoexcitation of iodide ion-pyrimidine clusters above the electron detachment threshold: Intracluster electron transfer *versus* nucleobase-centred excitations

Edward Matthews,[1] Rosaria Cercola,[1] Golda Mensa-Bonsu,[1] Daniel M. Neumark,[2] and Caroline E. H. Dessent[1]*

1 Department of Chemistry, University of York, Heslington, York, YO10 5DD, UK.

2 Department of Chemistry, University of California, Berkeley, CA 94720, USA, and Chemical Sciences Division, Lawrence Berkeley National Laboratory, Berkeley CA 94720, USA

ABSTRACT

Laser photodissociation spectroscopy of the I^-·thymine (I^-·T) and I^-·cytosine (I^-·C) nucleobase clusters has been conducted for the first time across the regions above the electron detachment thresholds to explore the excited states and photodissociation channels. Although photodepletion is strong, only weak ionic photofragment signals are observed, indicating that the clusters decay predominantly by electron detachment. The photodepletion spectra of the I^-·T and I^-·C clusters each display a prominent dipole-bound excited state (**I**) in the vicinity of the vertical detachment energy (~4.0 eV). Like the previously studied I^-·uracil (I^-·U) cluster [Li et al, J Chem Phys 145, 044319, (2016)], the I^-·T cluster also displays a second excited state (**II**) centred at 4.8 eV, which we similarly assign to a π–π∗ nucleobase-localized transition. However, no distinct higher-energy absorption bands are evident in the spectra of the I^-·C. TDDFT calculations are presented showing that while each of the I^-·T and I^-·U clusters display a single, dominant π–π∗ nucleobase-localized transition, the corresponding π–π∗ nucleobase transitions for I^-·C are split across three separate, weaker electronic excitations. I^- and deprotonated nucleobase anion photofragments are observed upon photoexcitation of both I^-·U and I^-·T, with the action spectra showing bands (at 4.0 and 4.8 eV) for both the I^- and deprotonated nucleobase anion production. The photofragmentation behaviour of the I^-·C cluster is distinctive as its I^- photofragment displays a relatively flat profile above the expected vertical detachment energy. We discuss the observed photofragmentation profiles of the I^-·pyrimidine clusters, in the context of the previous time-resolved measurements, and conclude that the observed photoexcitations are primarily consistent with intracluster electron transfer dominating in the near-threshold region, while nucleobase-centred excitations dominate close to 4.8 eV. TDDFT calculations suggest that charge-transfer transitions (Iodide n ($5p^6$) → Uracil σ*) may contribute to the cluster absorption profile across the scanned spectral region, and the possible role of these states is also discussed.

I. INTRODUCTION

It is well established that ionizing radiation and high-energy particles passing through biological material can efficiently produce low-energy secondary electrons.[1,2] These low-energy electrons are biologically important as they can cleave single- and double-DNA strands, as well as promote fragmentation in the constituent building blocks of DNA.[3-10] A broad range of experimental and theoretical studies have been conducted to characterise these processes at the molecular level, where the low-energy electron interacts directly with components of DNA. These studies have identified the unoccupied low-lying π^* orbitals of the nucleobases and the dissociative σ^* phosphate orbitals as possible sites for electron capture prior to transient negative ion formation.[9,10]

One novel approach for studying low-energy electron molecule coupling employs gas-phase iodide ion-molecule clusters, where the iodide ion is photodetached to produce low-energy free electrons with well-defined energies.[11-18] The free electrons can then be captured by the adjacent molecule to form a temporary negative ion, with the subsequent dynamics being probed either via photofragment action spectroscopy or time-resolved photoelectron spectroscopy.[11-18] In recent work, we studied the photodissociation dynamics of the iodide ion-uracil system ($I^-\cdot U$) to more closely investigate the role played by the "spectator" iodine.[18] Our $I^-\cdot U$ study revealed that photoexcitation produced I^- ion photofragments and, at lower signal levels, deprotonated nucleobase, i.e. $[U-H]^-$, photofragments, along with electron production from decay of a transient negative ion. The production spectra for both fragment ions displayed two peaks centred at ~4.0 and ~4.8 eV, with the lower-energy band being assigned to excitation of a dipole-bound excited state of the complex, while the higher-energy band was primarily assigned to excitation of a uracil-localized π-π^* transition. Although these two electronic excited states are quite distinctive in nature, time-resolved photoelectron imaging (TRPEI)

measurements indicated that across both bands, the I^- ion was being produced *via* internal conversion of the initially formed excited states back to the I^-·U electronic ground state followed by I^- evaporation. It was not possible to measure the TRPEI of the $[U-H]^-$ fragment dynamics due to the relatively low intensity of the ion.

Here, we extend our work on I^-·U to the other pyrimidine nucleobases (thymine and cytosine) to investigate the generality of the earlier results, focusing on the ionic fragments that are produced following near-threshold photoexcitation. As for I^-·U, the I^-·T cluster has also been investigated with TRPEI to investigate the electron loss channels,[16,17] however, the ionic photofragments that accompany near-threshold photoexcitation were not characterised in that study so this is the first direct investigation of the I^-·T photofragment channels. Moreover, the current work represents the first photoexcitation study of the I^-·C cluster. In particular, by comparing the photoexcitation spectra of these three nucleobase complexes, we aim to investigate the extent to which the intrinsic electronic characteristics of the nucleobase influence the cluster spectra, and hence to what extent the electronic excitations that occur can be described as nucleobase-localized transitions.

II. METHODS

UV photodissociation experiments were conducted in an AmaZon (Bruker) ion-trap mass spectrometer that has been converted for laser experiments as described in detail elsewhere.[19,20] The I^-·M clusters were generated by electrospraying solutions of nucleobase and iodide in deionized water (nucleobase solutions were 1×10^{-4} mol dm^{-3}, mixed with droplets of t-butyl ammonium iodide (TBAI) at 1×10^{-2} mol dm^{-3}). All chemicals were purchased from Sigma Aldrich and used without further purification.

The $I^-\cdot M$ clusters were mass-selected and isolated in an ion-trap prior to laser irradiation. UV photons were produced by an Nd:YAG (10 Hz, Surelite) pumped OPO (Horizon) laser across the range 345 - 230 nm (3.6 – 5.4 eV). Scans were conducted using a 1 nm step size. The total absorbance of the clusters is presented as photodepletion, which is calculated as the logarithm of the ratio between the ion intensity of mass-selected $I^-\cdot M$ clusters without and with irradiation. Photodepletion and photofragment production are corrected for laser power as described in references 19 and 20.

The structure of the $I^-\cdot M$ (M = uracil, thymine, cytosine) clusters was studied as part of this work using Gaussian 09.[21] Cluster structures of the iodide ion coordinated to known tautomers of the nucleobases were optimised using the B3LYP functional with the 6-311++G(2d,2p) basis set on C, N, O and H atoms and 6-311G(d,p) on I.[22-26] The core electrons of the iodide ion were described using the Stuttgart/Dresden (SDD) electron core pseudopotential.[27] Frequency calculations were performed after all geometry optimisations to ensure that all optimised structures correspond to true energy minima. Time-dependent density functional theory (TDDFT) calculations were performed on the lowest-energy optimised tautomer of the $I^-\cdot M$ clusters at the level described above. Dipole moments were calculated at the MP2/6-311++G(2d,2p) level, 6-311G(d,p)/SDD on I. The TDDFT method we have chosen to employ here for the excited state calculations follows those used recently by Noguchi et al. and Støckel et al. in their calculations of excited states of the luciferin anion.[28,29]

III. RESULTS

a. Geometric Structures and TDDFT calculations of the $I^-\cdot M$ clusters

Figure 1 (a-c) displays the most stable tautomer of each of the $I^-\cdot M$ (M = Uracil, Thymine, Cytosine) clusters, calculated at the B3LYP/6-311++G(2d,2p) level, 6-311G(d,p)/SDD on I.

For all of the I^-·M clusters, the most stable structure has the nucleobase in its biologically active form (keto-amino tautomer), with the iodide ion hydrogen-bonding to NH or CH bonds of the nucleobase, within the plane of the nucleobase. In this orientation, the iodide ion is bound along the axis of the permanent electric dipole moment of the isolated nucleobase. The calculated geometric structures of the I^-·U and I^-·T clusters are in good agreement with the structures presented in reference 16, obtained at the ωB97XD/aug-cc-pVDZ/aug-cc-pVDZ-pp level. To check that these structures do indeed correspond to the lowest-energy isomers, further calculations were conducted of a selection of cluster isomers with different nucleobase tautomers. These structures are presented in Section S1 of the supplementary material, and confirm that the structures presented in Figure 1 are the global minima at this level of theory. However, for I^-·C, a second cluster isomer (Isomer **2** in Table S3), which contains cytosine as the amino-oxo N3H tautomer, lies only 3.9 kJ/mol higher in energy than the global minimum isomer. We therefore anticipate that both Isomers **1** and **2** may be present in our experiment following electrospray ionization.[30,31] The presence of two isomers for I^-·C is perhaps unsurprising given that cytosine is known to exist in two tautomeric forms in the gas-phase.[32-34]

Table 1 lists the calculated electron detachment energies of the I^-·M clusters as well as cluster binding energies and dipole moments of the bare nucleobases. The values presented in Table 1 show that the calculations overestimate the VDEs of the I^-·U and I^-·T clusters by ~0.18 eV. If this trend is consistent across the nucleobases, we would expect the experimental VDEs of Isomers **1** and **2** of I^-·C to be ~3.95 eV, and ~4.01 eV, respectively. For all three I^-·M global minima clusters, the binding energies of the iodide to the nucleobase are similar. This is consistent with the calculated cluster structures, each of which involves two iodide ionic-hydrogen bonds. Table 1 also lists the calculated vertical dipole moments of the clusters (i.e.

the dipole moment of the neutral cluster ensemble calculated at the geometry of the ground state anion). We note that all three neutral vertical cluster structures are sufficiently polar to form stable dipole-bound anions.[35-37]

TDDFT calculations were conducted to complement the ground state calculations presented above, with the calculated excitation spectra for the I^-·M clusters being displayed in Figure 2. The calculated transitions energies and transition assignments are included in Section S2 of the supplementary material. Further benchmarking TDDFT calculations of the I^-·M clusters are available in the supplementary material and in reference 38. These TDDFT calculations are not expected to accurately predict the transition intensities of dipole-bound excited states, since the accurate calculation of such states is known to require the addition of tailored, diffuse functionals centred on the dipole-bound orbital.[39-41] We note that any electronic excitations that appear above the electron detachment threshold of the cluster will be resonance states rather than bound excited states.[42,43] The accurate theoretical prediction of such states is demanding, and beyond the scope of the current experimentally-focused work. Nonetheless, the calculations conducted here provide a guide for interpreting the experimental results, and follow on from other recent studies where TDDFT calculations have been successfully used to interpret experimental results for similar anionic systems.[28,29]

b. Photodepletion of the I^-·M (M = U, T, C) clusters

Figure 3 displays the photodepletion spectra of the I^-·M (M = uracil, thymine and cytosine) clusters measured across the range 3.6-5.4 eV. These spectra correspond to gas-phase absorption spectra in the limit where the excited states do not decay without fluorescence. The spectra shown in Figure 3 are broadly similar for each of the I^-·M clusters, with absorption onsets at 3.7 eV for the I^-·U and I^-·T clusters and a slightly lower onset of ~3.6 eV for I^-·C. All

of the photodepletion spectra display an absorption band (labelled **I**) between 3.7 – 4.2 eV that peaks at 4.0 eV for the I^-·U and I^-·T clusters, and at a slightly lower value of 3.9 eV for the I^-·C cluster.

Above the first absorption band (**I**), the absorption cross section increases fairly gradually from 4.2 – 5.4 eV for the I^-·U cluster (Figure 5a). The I^-·C cluster displays a very similar photodepletion profile, with a photodepletion cross section that increases gradually across the same range (Figure 4c). However, the I^-·T photodepletion spectrum is distinctive as it shows a more prominent and broad absorption band that peaks between 4.6 – 5.0 eV (Figure 5b). We next turn to characterizing the photofragmentation channels across the I^-·M cluster series to provide a fuller picture of the cluster photophysics, and the different decay pathways followed by the clusters after photoexcitation.

c. Photofragmentation of the I^-·M (M = U, T, C) clusters

Photofragment mass spectra of the I^-·M clusters (M = uracil, thymine and cytosine) irradiated at 3.95 eV (in the regions of the band **I** maxima) are presented in Figure 4. The mass spectra show that at this photoexcitation energy, all of the clusters photofragment with production of of I^-. In addition, the deprotonated nucleobase, $[M-H]^-$, is also observed as a minor photofragment for all three clusters at approximately 5, 3 and 1% of the intensity of the I^- photofragment for the uracil, thymine and cytosine clusters, respectively. We note that the deprotonated cytosine fragment appears only very weakly. (i.e. $[C-H]^-$ is approximately ten times weaker than the $[T-H]^-$ photofragment) in terms of ion counts accumulated under the same experimental measurement conditions. In comparison to other molecular systems we have studied in this instrument, the ionic photofragment intensity observed for the I^-·M clusters is low despite the strong photodepletion cross sections. This indicates that photodepletion of

these clusters across the range scanned is largely associated with pathways that result in electron detachment.

Figure 5 displays the I^- photofragment production spectra for the I^-·M clusters. The I^-·U and I^-·T clusters both fragment to produce I^- within two bands (labelled **I** and **II**) which peak at 3.95 and 4.77 eV for I^-·U, and 3.92 and 4.71 for I^-·T. The I^- production spectrum from I^-·C (Figure 4c) displays an onset at 3.8 eV, and again peaks in the band **I** region at 3.8 eV (band **I**). Above 4.0 eV, the I^- photofragment from I^-·C is produced with a continuous, flat profile and lacks the peak in production around 4.8 eV seen when I^- is produced from the I^-·U and I^-·T clusters.

Production spectra of the $[M-H]^-$ photofragments are included in Section S3 of the supplementary material. For I^-·U and I^-·T, the $[M-H]^-$ photofragments are produced within the same absorption bands (**I** and **II**) as the I^- photofragment (Figure 5a and 5b). In comparison to the I^- photofragment spectra, the relative intensities of bands **I** and **II** are broadly similar for the $[U-H]^-$ and $[T-H]^-$ photofragments, although the $[U-H]^-$ is produced somewhat more strongly through band **I** than band **II** in comparison to the I^- photofragment (Figure 5a) for the I^-·U cluster. The $[C-H]^-$ photofragment is produced very weakly throughout the scanned spectral range for the I^-·C cluster, although there is some enhancement in the photofragment signal between 3.7 - 4.3 eV, i.e. across the band **I** region.

IV. DISCUSSION

a. General overview of photodecay channels

Photoexcitation of an I^-·M cluster can lead to excited state decay by a number of different pathways. In the absence of fluorescence, all of these channels will contribute to the total

photodepletion cross section. Ionic photofragmentation is energetically possible via one of three routes:

$$I^-\cdot M \rightarrow I + M^- \quad [1a]$$

$$\rightarrow I^- + M \quad [1b]$$

$$\rightarrow HI + [M\text{-}H]^- \quad [1c]$$

Electron detachment at energies above the electron detachment energy of the cluster is possible either via direct detachment [2a] or indirect processes that arise from various excited states of the cluster ([2b]),[16] or from "hot" photofragments ([2c] or [2d]):

$$I^-\cdot M \rightarrow I\cdot M + e^- \quad [2a]$$

$$\rightarrow [I\cdot M]^{*-} \rightarrow [I\cdot M] + e^- \quad [2b]$$

$$\rightarrow I + M^{*-} \rightarrow I + M + e^- \quad [2c]$$

$$\rightarrow HI + [M\text{-}H]^{*-} \rightarrow HI + [M\text{-}H] + e^- \quad [2d]$$

As noted above, the ionic photofragments are produced with very low intensities across the spectral range studied here, so the primary conclusion in terms of the photodissociation dynamics is that electron detachment channels dominate. Indeed, the spectral profiles for the summed electron detachment channels for all three $I^-\cdot M$ clusters (Figure S13 in the supplementary material) closely resemble the photodepletion spectra (Figure 3).

b. On the nature of the excited states observed for the $I^-\cdot M$ clusters

The 4.0 eV absorption band (**I**) present in the photodepletion spectra of the $I^-\cdot U$ and $I^-\cdot T$ clusters, peaks just below the experimental VDEs of 4.11 and 4.05 eV, respectively.[16] It has been previously established for these clusters that dipole-bound excited states can be accessed

at photon energies slightly below the electron detachment threshold,[16-18] so that the 4.0 eV band for the $I^-\cdot U$ and $I^-\cdot T$ clusters can be confidently assigned to excitation of a dipole-bound excited state. Indeed, we have found clear evidence for the formation of dipole-bound excited states within our laser-interfaced mass spectrometry instrument following near-threshold excitation of anionic salt clusters ($I^-\cdot MI$ where M = Na, K, Cs),[44] and are therefore confident that these states can be observed using our experimental method. The absorption spectrum of the $I^-\cdot C$ cluster in the vicinity of band **I** strongly resembles the absorption spectra of the $I^-\cdot U$ and $I^-\cdot T$ clusters, displaying a prominent absorption band in the spectral region where the VDE of the cluster is expected to occur. (From the calculations shown in Table 1, the VDEs of isomers **1** and **2** of $I^-\cdot C$ would be expected to occur around 3.95 and 4.01 eV.) This leads us to assign the 3.9 eV centred absorption band (**I**) of $I^-\cdot C$ to a dipole-bound excited state.

We next turn to considering the nature of the iodide-nucleobase cluster excited state(s) accessed in the region around 4.8 eV. In our recent study of the photodissociation dynamics of $I^-\cdot U$, we identified a second cluster excited state (~4.8 eV) which we assigned to a cluster transition that was associated with a π-π^* transition localized on the uracil moiety.[18] This band, labelled **II**, can be seen most clearly in the photofragment action spectra (e.g. the I^- action spectrum from $I^-\cdot U$ displayed in Fig. 5a). Comparing the spectra obtained in this work for $I^-\cdot T$ to those for $I^-\cdot U$, we can again assign a second excited state (**II**) for the $I^-\cdot T$ cluster. This excited state is visible in the photofragment action spectra, centred at ~4.75 eV (e.g. in the I^- photofragment action spectrum in Fig. 5b). We note that these excited states are resolved in the photofragment action spectra but not in the photodepletion spectra since the photodepletion spectra include contributions from direct electron detachment [2a] above the cluster detachment threshold. For the $I^-\cdot C$ cluster, however, no resolved band **II** is evident in the I^- photofragment action spectrum.

The TDDFT results presented in Section IIIa provide some insight into the electronic spectra of the $I^-\cdot M$ clusters. For all three clusters, a number of charge-transitions associated with the iodide p-orbitals (Iodide n ($5p^6$) → Uracil σ*) are predicted across the spectral range studied here. All of these orbitals are diffuse in nature, but with some orbital density remaining on the molecular framework, thus indicating that they have significant dipole-bound character. In addition, for $I^-\cdot U$ and $I^-\cdot T$, a single dominant transition is predicted associated with a π-orbital nucleobase-localised transition. This transition occurs in the region of the experimentally observed band **II** features, at 5.04 and 4.86 eV for $I^-\cdot U$ and $I^-\cdot T$, respectively. The TDDFT calculations predict electronic transitions for Isomer **1** of $I^-\cdot C$ that differ from those of $I^-\cdot U$ and $I^-\cdot T$ as there are three much lower-intensity π-orbital nucleobase-localised transitions predicted for the cytosine cluster at 4.77, 5.22 and 5.43 eV. Thus the TDDFT calculations provide an explanation for the differing nature of the experimentally observed electronic spectrum of $I^-\cdot C$ compared to $I^-\cdot U$ and $I^-\cdot T$. Whereas the transition intensity for nucleobase-π-orbital transitions in $I^-\cdot U$ and $I^-\cdot T$ is localized in a single strong transition, producing a prominent band **II** feature for each of these clusters, in isomer **I** of $I^-\cdot C$, this transition intensity is distributed across several transitions so that no single band **II** feature is evident. (In uncomplexed gaseous cytosine, weak transitions have been recorded for the keto-amino tautomer as low as ~4 eV.[33,34,45,46]) Moreover, if the second $I^-\cdot C$ isomer (**II**) is also present in the experiment, then this may contribute to further distribute the transition intensity, since this isomer displays a pair of nucleobase-localized transitions at 4.45 and 5.65 eV (Figure 2d).

The fact that the TDDFT calculated spectra of the $I^-\cdot M$ clusters with respect to the nucleobase-localized transitions, appear to do a good job of predicting the main features of the photodepletion/photofragment action spectra indicates that nucleobase-localized transitions are the primary excitations controlling the main differences in the photodepletion profiles over the

4.2-5.2 eV region. We note that the charge-transfer transitions (Iodide n ($5p^6$) → Uracil σ*) are predicted to make significant contributions to the overall absorption profiles of the clusters. Molecular orbitals involved in the TDDFT excitations for I^-·U and I^-·C (amino-oxo-N1H tautomer) are included in Section S3 of the Supplementary Material. We note that a particularly strong charge-transfer transition is predicted for the amino-oxo-N1H tautomer of I^-·C, and return to discussing the role of these states in Section IVd.

Finally, we turn to considering whether the two spin-orbit channels of iodine atom influence the overall appearance of the photodepletion and photofragmentation spectra. Direct detachment to the upper 2P1/2 neutral states of the I^-·T and I^-·U clusters was evident around 5 eV in the one-photon photoelectron spectra.[15] In a recent study of I^-·MI (M = Na, K, Cs) anionic salt microclusters conducted in one of our groups, the upper ($^2P_{½}$) spin-orbit state of the I^-·KI cluster was evident in the photodepletion spectrum ~0.94 eV above the lower ($^2P_{3/2}$) spin-orbit state.[44] However, the $[KI]^-$ photofragment spectrum that accompanies the photodepletion spectrum of this cluster revealed that no ionic photofragments were produced across the region of the upper spin-orbit state of the cluster. We concluded that the lack of photofragments resulted from rapid spin-orbit relaxation of the upper iodine $^2P_{½}$ state accompanied by electron detachment occurring on a timescale that is faster than decay to ionic photofragments. Such dynamics had been previously observed for other iodide ion-molecule complexes by Mabbs and coworkers, who have reported that the photodetachment dynamics in the vicinity of the $^2P_{½}$ state threshold are strongly correlated with the molecular dipole.[47] Consideration of these previous studies leads us to conclude that the upper spin-orbit dipole-bound state of the iodide ion-pyrimidine clusters studied here is not evident in the photodepletion spectra due to it occurring with a relatively low cross section (akin to I^-·CH_3CN),[48] and hence being obscured by the nucleobase-centred excitations that occur over

the same region. Any accompanying photofragments would also therefore be produced with low cross-section, but may indeed not be observed at all as in the I^-·KI system.[44]

c. On the distinctive electron detachment profile of the I^-·T cluster

One notable difference between the photodepletion spectra of I^-·T compared to I^-·U and I^-·C is the much larger cross section for photodepletion that is evident between 4.2-5.2 eV. Given that this feature is uniquely observed in the I^-·T photodepletion spectrum, the enhanced photodepletion appears to be linked to transitions centred on the thymine moiety. However, as discussed in Section 4a, photodepletion for all three clusters is predominantly associated with electron loss decay channels, so that a [2b] - [2d] type process must be occurring, consistent with an enhanced probability for excitation to a dissociative or autodetaching state of the anion.

This situation is reminiscent of behaviour we observed in photoelectron spectroscopy of $PtCl_6^{2-}$·T clusters, where indirect electron emission was observed from the cluster following 266 nm photoexcitation.[49] The indirect electron emission is indicative of autodetachment of the anionic cluster excited state or dissociative products. Given that the enhanced propensity for electron detachment is centred around 4.7 eV, it seems highly probable that the state involved is a thymine-localized π-π* excitation, or can be accessed by evolution of this state. It is important that enhanced electron emission has been seen following 4.7 eV excitation for both the singly-charged I^-·T and the multiply-charged $PtCl_6^{2-}$·T. While 4.7 eV excitation of I^-·T could in principle produce an ~0.7 eV free electron that could be captured by the thymine to form a valence anion, i.e.

$I^-\cdot T \rightarrow I\cdot T^-_{VBS}$

such a process is not possible from the multiply charge cluster due to the presence of repulsive coulomb barriers on the potential energy surface, so that any free electrons are generated with significant kinetic energy.

d. On the mechanism of photofragment production

Ionic photofragments can be formed by two general mechanisms. The first group of mechanisms can be broadly described as intracluster electron transfer, and includes processes that follow either dipole-bound excited state formation, ejection of a low energy electron from the I^- that subsequently undergoes electron scattering with the nucleobase or direct charge transfer from I^- to the valence orbitals of the nucleobase. These process would be expected to result in production of either the dipole-bound anion of the nucleobase, M^- (following direct decay of the dipole-bound excited state) or, the deprotonated nucleobase anion, $[M-H]^-$. The second type of photofragmentation mechanism follows an electronic excitation that is largely localized on the nucleobase moiety. The pyrimidines are well known for their propensity to decay by ultrafast relaxation back to the ground electronic state following UV excitation, and then dissipate excess energy by thermal dissipation.[50-52] In $I^-\cdot M$ where a nucleobase-localized transition is excited, we would anticipate formation of fragments associated with dissociation of a hot electronic ground state.[53] Any such ionic fragments formed through thermal fragmentation of the electronic ground state system can be identified by conducting low-energy collision-induced dissociation on the $I^-\cdot M$ clusters in the quadrupole ion trap of our instrument.[20,55] On performing low-energy collision-induced dissociation, I^- was observed as the sole ionic fragment.

As discussed in Section IVb, we have assigned the ~4.0 and ~4.8 eV excited states of the $I^-\cdot M$ clusters to a dipole-bound state and a nucleobase-localised excited state, respectively, and

would simplistically have expected to see $[M-H]^-$ (or a nucleobase dipole-bound anion) as the photofragment from the ~4.0 eV excited state, and I^- as the photofragment from the 4.8 eV excited state. However, the photofragment mass spectra and photofragment action spectra for all three of the iodide-pyrimidine clusters clearly show the two photofragments are produced across both of these distinctive excited states. The inferred decay mechanisms have been discussed in detail in our recent paper on $I^-\cdot U$,[18] which included femtosecond time-resolved measurements. To summarise the conclusions of that paper, both the ~4.0 eV and 4.8 eV excited states were found to decay with long lifetimes for production of the I^- ion, consistent with internal conversion to the ground electronic state followed by evaporation of I^-. The $I^-\cdot T$ and $I^-\cdot C$ clusters studied in this work display similar propensities to produce I^- as a photofragment from both the 4.0 and higher energy nucleobase localized-excited states, along with the respective $[M-H]^-$ ion as a minor photofragment. This suggests that similar photodissociation dynamics are operating in all three clusters, although direct time-resolved measurements will be necessary to confirm this.

One of the intriguing aspects of the calculations performed as part of this study is that Iodide n ($5p^6$) → Uracil σ* charge-transfer transitions are predicted to be reasonably strong in both the dipole-bound region of the spectra, and in the regions close to the nucleobase localized π→π* transitions. There are a number of aspects of the dynamics of the $I^-\cdot M$ complexes that were previously unexplained,[14-18] that may be attributed to these charge-transfer states. In particular, if the σ* and π* excited states are strongly coupled, an excitation of the σ* state may be evident as observed behaviour that is characteristic of the π* state, i.e. an observation of electron detachment from a valence-bound anion state in the photoelectron spectroscopy measurements. For example, the near-simultaneous rise of detachment signals from dipole-bound and valence-bound signals at excitation energies near the VDE could be readily explained if there is strong

σ* and π* coupling. This effect could also explain the instantaneous rise of valence-bound signals around 4.7 eV, which is very challenging to explain within a picture where only π→π* excitations occur at this energy. Of the other clusters studied in this work, the I^-·C (amino-oxo-N1H tautomer) displays particularly strong σ* and π* coupling for the TDDFT excitations that are predicted to occur at 5.22 and 5.27 eV (See Figures S8 and S11 of the Supplementary Information.). This suggests an alternative explanation for the distinctive photofragmentation behaviour of I^-·C as arising due to strong σ* and π* coupling across the above threshold region. Further theoretical work is clearly desirable to fully investigate the nature and role of these charge-transfer states in the photophysics of iodide-nucleobase complexes.

V. CONCLUSIONS

Laser photodissociation spectroscopy (3.5-5.4 eV) has been applied to investigate the dissociative channels of the I^-·M clusters following photoexcitation. The photodepletion spectra, equivalent to gas-phase absorption spectra, reveal the presence of two bands across this spectral region for I^-·U and I^-·T which we have assigned to a dipole-bound excited state (~4.0 eV) and a nucleobase-localized π-π* excitation (~4.8 eV). The primary photodecay channel from both (above threshold) excited states corresponds to electron loss, either via direct detachment or via indirect processes. Ionic photofragmentation channels are evident as minor processes, with photofragmentation producing I^- as the dominant ionic photofragment for each of the three clusters, with the corresponding action spectra displaying band maxima around 4.0 eV and 4.8 eV for both I^-·U and I^-·T. The behaviour of the I^-·C cluster is somewhat distinctive, as although a near threshold dipole-bound excited state is again evident, photofragment ion production is relatively flat across the spectral region scanned above the detachment energy. We attribute this to the presence of a relatively larger and weaker number of cytosine-localised electronic transitions associated with the I^-·C cluster, and suggest that this effect is likely

enhanced due to a second low-energy isomer (**2**) of the $I^-\cdot C$ cluster also being present in the experimental ensemble. Finally, we note that the calculations performed in this work suggest that strong σ^* and π^* coupling may exist in the cluster excited states. This situation should certainly be investigated using more rigorous theoretical treatments,[56-58] to provide a further understanding of the extent of orbital coupling and its impact on the excited state photophysics.

SUPLEMENTARY MATERIAL

The supplementary material includes DFT calculations on the tautomers of the $I^-\cdot M$ clusters, TDDFT studies of the $I^-\cdot M$ clusters, Molecular orbitals involved in the TDDFT transitions of $I^-\cdot$Uracil and the amino-oxo-N1H tautomer of $I^-\cdot$Cytosine, production spectra of the $[M-H]^-$ photofragments, and electron detachment action spectra.

ACKNOWLEDGMENTS

The work reported in this paper was initiated with financial support from the European Research Council Grant No. 208589-BIOIONS. DMN is supported by the National Science Foundation under Grant no. CHE-1361412. We also thank the University of York and the Department of Chemistry at the University of York for provision of funds for the Horizon OPO laser system, and the York Advanced Computing Cluster (YARCC) for access to computational resources. We also thank Dr Ananya Sen for early contributions to this project.

REFERENCES

[1] S. M. Pimblott and J. A. LaVerne, Radiat. Phys. Chem. **76**, 1244 (2007).

[2] L. Sanche, Radiat. Phys. Chem. **34**, 15 (1989).

[3] B. Boudaiffa, P. Cloutier, D. Hunting, M. A. Huels and L. Sanche, Science **287**, 1658 (2000).

[4] L. Sanche, Eur. Phys. J. D **35**, 367 (2005).

[5] J. K. Wolken and F. Turecek, J. Phys. Chem. A **105**, 8352 (2001).

[6] S. G. Ray, S. S. Daube and R. Naaman, Proc. Natl. Acad. Sci. U.S.A. **102**, 15 (2005).

[7] H. Abdoul-Carime, S. Gohlke and E. Illenberger, Phys. Rev. Lett. **92**, 168103 (2004).

[8] I. Baccarelli, I. Bald, F. A. Gianturco, E. Illenberger and J. Kopyra, Phys. Rep. **508**, 1 (2011).

[9] H. Abdoul-Carime, S. Gohlke, E. Fischbach, J. Scheike and E. Illenberger, Chem. Phys. Lett. **387**, 267 (2004).

[10] J. D. Gu, J. Leszczynski and H. F. Schaefer, Chem. Rev. **112**, 5603 (2012).

[11] C. E. H. Dessent, C. G. Bailey and M. A. Johnson, J. Chem. Phys. **105**, 10416 (1996).

[12] C. E. H. Dessent, J. Kim and M. A. Johnson, Faraday Discuss. **115**, 395 (2000).

[13] F. Mbaiwa, M. Van Duzor, J. Wei and R. Mabbs, J. Phys. Chem. A **114**, 1539 (2010).

[14] M. A. Yandell, S. B. King and D. M. Neumark, J. Am. Chem. Soc. **135**, 2128 (2013).

[15] S. B. King, M. A. Yandell, and D. M. Neumark, Faraday Disscuss. **163**, 59 (2013).

[16] S. B. King, M. A. Yandell, A. B. Stephansen and D. M. Neumark, J. Chem. Phys. **141**, 224310 (2014).

[17] S. B. King, A. B. Stephansen, Y. Yokoi, M. A. Yandell, A. Kunin, T. Takayanagi and D. M. Neumark, J. Chem. Phys. **143**, 024313 (2015).

[18] W. L. Li, A. Kunin, E. Matthews, N. Yoshikawa, C. E. H. Dessent and D. M. Neumark, J. Chem. Phys. **145**, 044319 (2016).

[19] E. Matthews, A. Sen, N. Yoshikawa, E. Bergstrom and C. E. H. Dessent, Phys. Chem. Chem. Phys. **18**, 15143 (2016).

[20] A. Sen, T. F. M. Luxford, N. Yoshikawa and C. E. H. Dessent, Phys. Chem. Chem. Phys. **16**, 15490 (2014).

[21] M. J. Frisch, G. W. Trucks, H. B. Schlegel *et al*., GAUSSIAN 09, Revision D.01, Gaussian, Inc., Wallingford, CT, 2009.

[22]A. D. Mclean and G. S. Chandler, J. Chem. Phys. **72**, 5639 (1980).

[23] R. Krishnan, J. S. Binkley, R. Seeger and J. A. Pople, J. Chem. Phys. **72**, 650 (1980).

[24]A. D. Becke, J. Chem. Phys. **98**, 5648 (1993).

[25]T. Clark, J. Chandrasekhar, G. W. Spitznagel and P. V. Schleyer, J. Comput. Chem. **4**, 294 (1983).

[26]M. J. Frisch, J. A. Pople and J. S. Binkley, J. Chem. Phys. **80**, 3265 (1984).

[27]A. Bergner, M. Dolg, W. Kuchle, H. Stoll and H. Preuss, Mol. Phys. **80**, 1431 (1993).

[28]Y. Noguchi, M. Hiyama, H. Akiyama, and Nobuaki Koga, J. Chem. Phys. **141**, 044309 (2014).

[29]K. Støchkel, B. F. Milne, and S. B. Nielsen, J. Phys. Chem. A **115**, 2155 (2011).

[30]E. Matthews and C. E. H. Dessent, Phys. Chem. Chem. Phys. **19**, 917434 (2017).

[31]E. Matthews and C. E. H. Dessent, J. Phys. Chem. A **120**, 9209 (2016).

[32]J. Schiedt, R. Weinkauf, D. M. Neumark and E. W. Schlag, Chem. Phys. **239**, 511 (1998).

[33]E. Nir, C. Plutzer, K. Kleinermanns and M. de Vries, Eur. Phys. J. D 20, 317 (2002).

[34]E. Nir, M. Muller, L. I. Grace and M. S. de Vries, Chem. Phys. Lett. 355, 59 (2002).

[35]O. H. Crawford and W. R. Garrett, J. Chem. Phys. **66**, 4968 (1977).

[36]O. H. Crawford, Mol. Phys. **20**, 585 (1971).

[37]W. R. Garrett, J. Chem. Phys. **77**, 3666 (1982).

[38]G. Mensa-Bonsu, MSc thesis, University of York, 2016.

[39]M. Gutowski and P. Skurski, J. Phys. Chem. A **102**, 2624 (1998).

[40]P. Skurski, M. Gutowski and J. Simons, Int. J. Quantum Chem. **80**, 1024 (2000).

[41]W. J. Morgan and R. C. Fortenberry, Theor. Chem. Acc. **134**, 47 (2015)

[42]J. Simons, J. Phys. Chem. A **112**, 6401 (2008).

[43]J. Simons, Annu. Rev. Phys. Chem. **62**, 107 (2011).

[44]A. J. A. Harvey, N. Yoshikawa, J. G. Wang and C. E. H. Dessent, J. Chem. Phys. **143**, 101103 (2015).

[45] L. B. Clark, G. G. Peschel and I. Tinoco, J. Phys. Chem. **69**, 3615 (1965).

[46]G. Bazso, G. Tarczay, G. Fogarasi and P. G. Szalay, Phys. Chem. Chem. Phys. **13**, 6799 (2011).

[47]F. Mbaiwa, D. Dao, N. Holtgrewe, J. Lasinski and R. Mabbs, J. Chem. Phys. **136**, 114303 (2012).

[48]R. Mabbs, E. Surber and A. Sanov, J. Chem. Phys. **122**, 054308 (2005).

[49]A. Sen, E. M. Matthews, G. L. Hou, X. B. Wang and C. E. H. Dessent, J. Chem. Phys. **143**, 184307 (2015).

[50]R. Improta, F. Santoro and L. Blancafort, Chem. Rev. **116**, 3540 (2016).

[51]M. Barbatti, A. J. A. Aquino, J. J. Szymczak, D. Nachtigallova, P. Hobza and H. Lischka, Proc. Natl. Acad. Sci. U.S.A. **107**, 21453 (2010).

[52]C. E. Crespo-Hernandez, B. Cohen, P. M. Hare and B. Kohler, Chem. Rev. **104**, 1977 (2004).

[53]We note that excited state decay processes for iodide-molecule complexes are not always ergodic. Reference [54] presents an example.

[54] A. Kunin, L. L. Li, and D. M. Neumark, Phys. Chem. Chem. Phys. **18**, 33226 (2016).

[55] R. Cercola, E. Matthews, and C. E. H. Dessent, J. Phys. Chem. B, **121**, 5553 (2017).

[56] T. Sommerfeld and M. Ehara, J. Chem. Phys. **142**, 034105 (2015).

[57]Y. Kanazawa, M. Ehara and T. Sommerfeld, J. Phys. Chem. A **120**, 1545 (2016).

[58]T.C. Jagau, K. B. Bravaya and Anna I. Krylov, Annu. Rev. Phys. Chem. **68**, 525 (2017).

TABLES

Table 1: Vertical detachment energies (VDE), adiabatic electron affinities (AEA), cluster binding energies and nucleobase dipole moments. VEDs and ADEs are calculated at the B3LYP/6-311++G(2d,2p)/SDD level, while the vertical dipole moments were calculated at the MP2/6-311++G(2d,2p)/SDD level.

Structure	**I^-·U**	**I^-·T**	**I^-·C (1)**	**I^-·C (2)**
Experimental VDE (eV)[a]	4.11	4.05	-	-
Calculated VDE (eV)	4.30	4.22	4.13	4.16
Calculated ADE (eV)	4.20	4.14	3.85	4.13
Cluster Binding Energy (kJ mol^{-1})	98.6	93.9	86.3	110.4
Nucleobase Dipole Moment (D)	6.19	5.97	8.36	9.47

a – Experimental VDEs taken from reference 15.

FIGURES

Figure 1: Global minima geometric structures of the $I^-\cdot M$ clusters, where M= a) uracil, b) thymine and c) cytosine. Clusters were optimised at the B3LYP/6-311++G(2d,2p) level.

Figure 2 TDDFT excitation spectra of the $I^-\cdot M$ clusters, where M = a) uracil, b) thymine, c) amino-oxo-N1H cytosine and d) amino-oxo-N3H cytosine. The red lines correspond to transitions originating from an iodide p-orbital. The blue lines correspond to transitions originating from a nucleobase π orbital. The full line spectrum represents a convolution of the calculated electronic transitions with Gaussian functions (0.25 eV HWHM).

Figure 3: Photodepletion spectra of the $I^-\cdot M$ clusters across the range 3.5 – 5.4 eV, where M = a) uracil, b) thymine and c) cytosine. The solid red lines are five-point adjacent averages of the data points. Part a) of this Figure is reproduced from W. L. Li, A. Kunin, E. Matthews, N. Yoshikawa, C. E. H. Dessent and D. M. Neumark, J. Chem. Phys. **145**, 044319 (2016), with the permission of AIP publishing.

Figure 4: Photofragment mass spectra of the a) $I^-\cdot U$, b) $I^-\cdot T$ and c) $I^-\cdot C$ clusters photoexcited at 3.95 eV (314 nm). The intensities of the ions are given as a percentage of the intensity of the parent $I^-\cdot M$ cluster without irradiation. The $I^-\cdot M$ cluster is denoted by an *. The inset on each spectrum shows the intensity of the deprotonated nucleobase ($[M-H]^-$) fragment.

Figure 5: Photofragment production spectra of I^- produced by the $I^-\cdot M$ clusters across the range 3.5 – 5.4 eV, where M = a) uracil, b) thymine and c) cytosine. The solid red lines are five-point adjacent averages of the data points. Part a) of this Figure is reproduced from W. L. Li, A. Kunin, E. Matthews, N. Yoshikawa, C. E. H. Dessent and D. M. Neumark, J. Chem. Phys. **145**, 044319 (2016), with the permission of AIP publishing.

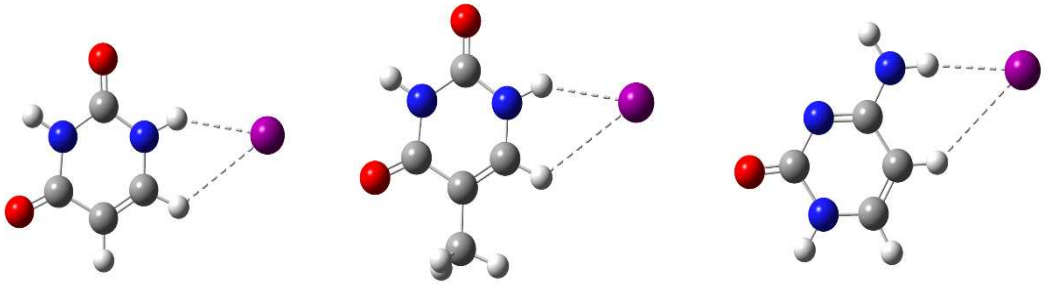

I II III

Figure 1

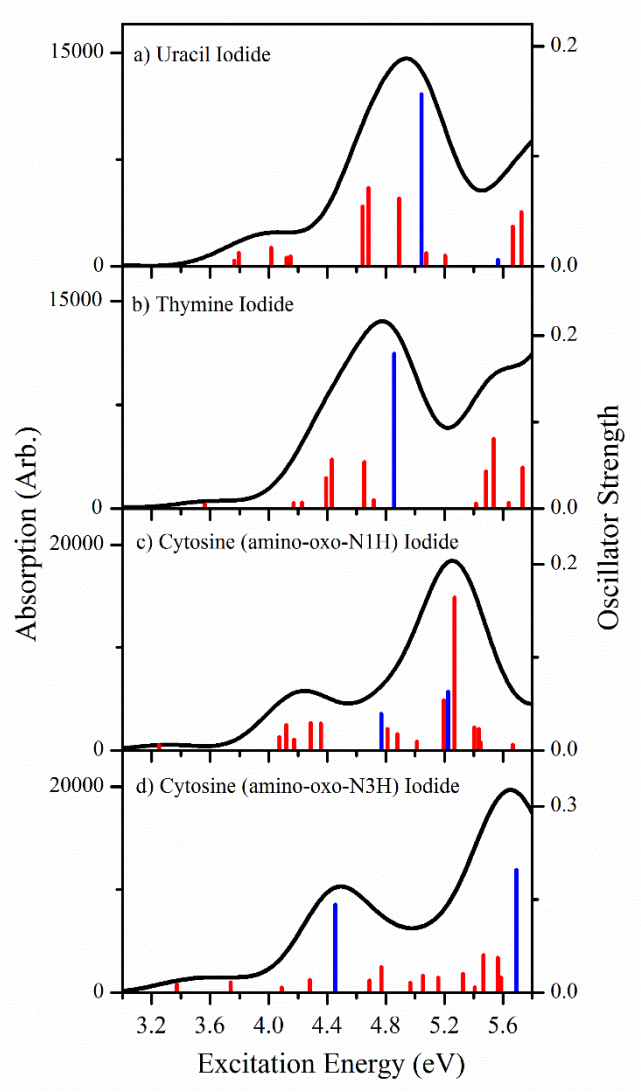
a) Uracil Iodide
b) Thymine Iodide
c) Cytosine (amino-oxo-N1H) Iodide
d) Cytosine (amino-oxo-N3H) Iodide
15000
0
20000
0.2
0.0
0.3
Absorption (Arb.)
Oscillator Strength
3.2
3.6
4.0
4.4
4.8
5.2
5.6
Excitation Energy (eV)

Figure 2

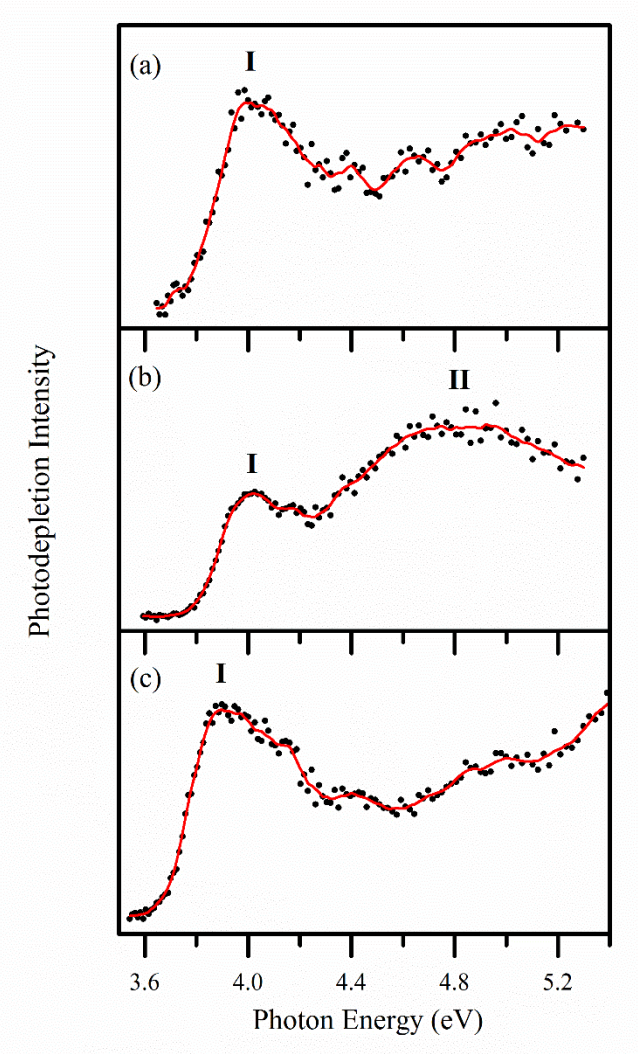
(a)
I
(b)
II
I
(c)
I
Photodepletion Intensity
3.6
4.0
4.4
4.8
5.2
Photon Energy (eV)

Figure 3

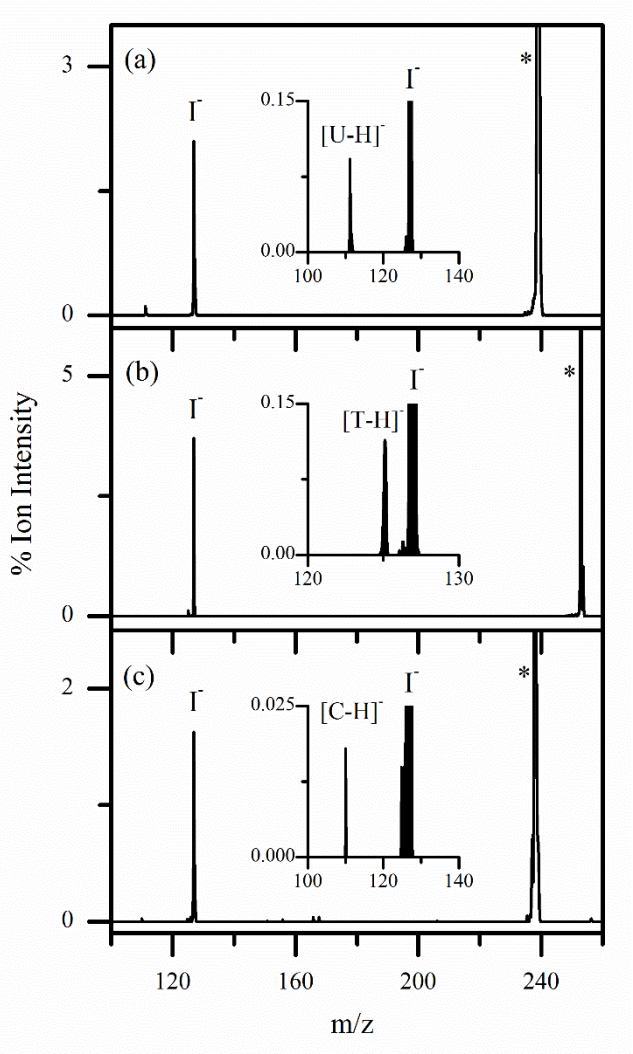
(a)
(b)
(c)
I-
[U-H]-
[T-H]-
[C-H]-
*
% Ion Intensity
m/z
3
0
5
2
120
160
200
240
0.15
0.00
0.025
0.000
100
120
130
140

Figure 4

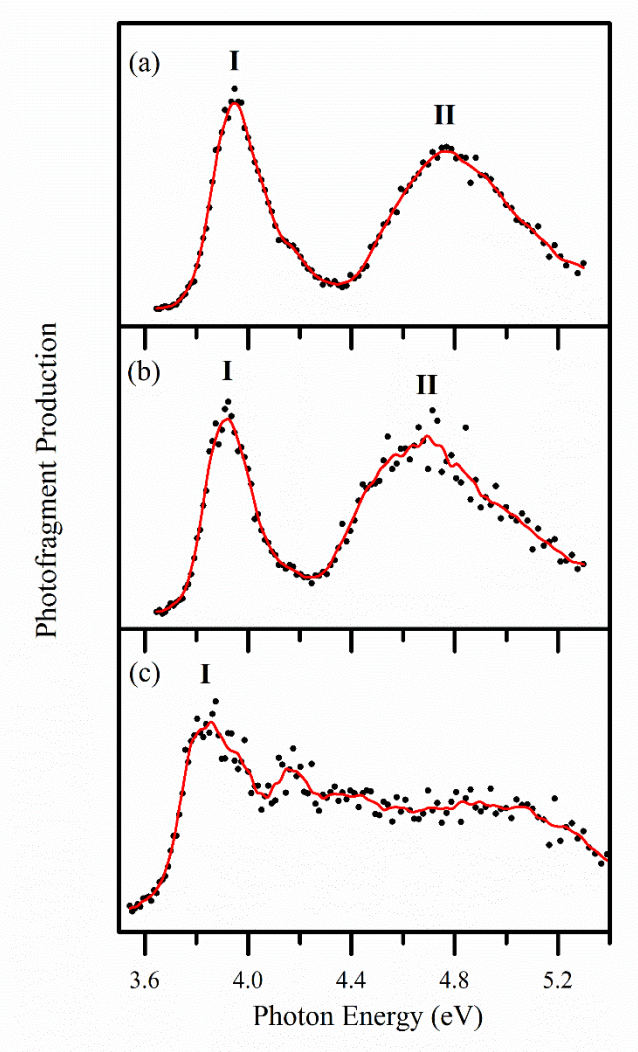
(a)
I
II
(b)
I
II
(c)
I
Photofragment Production
3.6
4.0
4.4
4.8
5.2
Photon Energy (eV)

Figure 5